3D-Modeling of a Coaxial Borehole Heat Exchanger in Sahand Field, Northwest Iran Considering the Porous Medium and Presence of Nanofluids

Mehrpooya, Mehdi[*+•]*; Ghafoorian, Farzad; Farajyar, Shayan*

Hydrogen and fuel cell laboratory, Faculty of New Sciences and Technologies, University of Tehran, Tehran, I.R. IRAN

ABSTRACT: *The purpose of this study is the 3D CFD numerical modeling of a coaxial borehole heat exchanger. The operating fluid inlet velocity, the groundwater seepage velocity, the soil porosity, and the use of nanofluids instead of pure water are investigated. Ansys Fluent software is used for numerical simulation and the k-ε turbulence model is employed for turbulent flow modeling. The results show that they significantly increase the operating fluid temperature. The presence of groundwater seepage decreases the temperature of the working fluid which is related to the groundwater flow velocity. High soil and backfill porosity affect the thermal performance of CBHE and increase thermal resistance and decrease thermal conductivity. The nanofluids utilization with a higher thermal conductivity than pure water increases the temperature growth rate along the outer pipe. Kriging optimization method suggested that the best operating conditions for the system are inlet water velocity 0.03 m/s, groundwater velocity 5 m/d, soil porosity 0.28, backfill thermal conductivity 3.3 (W/m.K) and CuO/water nanofluid. By considering the mentioned operating conditions, the working fluid temperature increases by about 6% at the depth of 60 m.*

KEYWORDS: *Coaxial borehole heat exchanger; Computational fluid dynamics; Groundwater seepage; Soil porosity; Nanofluid.*

INTRODUCTION

Rising concerns about global warming and pollution of the environment have led to a growing interest in renewable energy. Sources of clean fuels such as wind, solar, hydropower, geothermal, and biomass are alternatives to fossil fuels. In recent years, one of the ways to use geothermal energy is the Ground Source Heat Pump (GSHP), which many researchers have considered [1]. Borehole Heat Exchangers (BHE) are one of the main components of geothermal heat pumps commonly applied to save energy in warming and chilling buildings [2]. Different geometries are used for borehole heat exchangers and concentric heat exchanger is widely used [3,4]. Abandoned and old oil and gas wells can be used as geothermal sources. Scientists simulated a coaxial geothermal heat exchanger on two abandoned oil wells in Ahvaz and compared the efficiency of using these two

sources [5]. In this system, the exteriority between the ground and the external pipe of CBHE can be filled with grout. In some special models, a CBHE does not need to be filled with cement, and the surface of the outer pipe is connected directly to the soil [6]. In general, heat pumps in combination with other renewable energy extraction equipment, including solar panels, are widely used in Iran [7]. A numerical study on the temperature changes and efficiency of a U-shaped geothermal heat exchanger was applied in that study, and the presence of groundwater was considered [8]. It was also found that the soil and material type used for backfill, which has different physical and thermal properties, have a significant effect on the thermal performance of the BHE system [9]. Groundwater temperature changes across soil width were evaluated, and the effects of groundwater seepage at different velocities and directions on the efficiency of the U-shaped heat exchanger were considered [10]. The study on the different inner pipe geometrical configurations on the performance of the double-pipe heat exchanger showed that a flat inner pipe at a low Reynolds number boosted the performance [11]. In a numerical study on different types of BHEs, the effects of groundwater seepage into saturated soil with different velocities and flow rates at certain depths were determined, and it was found that the presence of groundwater seepage can reduce the thermal efficiency of the BHE [12,13]. It should be noted that groundwater intrusion strongly depends on the percent of soil porosity and the soil layer [14]. Also, the results of non-Darcy modeling have shown that the porous medium and the thickness of its layers have a significant effect on increasing the buoyancy forces and subsequently increasing the temperature gradient [15]. Another parameter affecting the increase in temperature changes along the inlet pipe is the variation of velocity or volumetric flow rate of the inlet [16]. The results showed that by decreasing the velocity or inlet volume flow rate, temperature changes along the pipe increased [17]. The thermal conductivity of working fluid has a significant impact on thermal efficiency, and the use of different nanofluids or gases can provide it [18]. As Brownian motion increases, the thermal conductivity increases with temperature. For example, Al_2O_3/Water and CuO/Water were studied and it was observed that the thermal conductivity reaches a peak with temperature [19]. Pure water was replaced with CuO/Water and Al_2O_3/Water

nanofluids in the inlet pipe of a coaxial heat exchanger, resulting in a greater temperature difference along the pipe. Furthermore, CuO/Water nanofluid further improved thermal performance than Al_2O_3/Water [20]. The effect of different nanofluids with different volume fractions on improving thermal parameters in a U-shaped geothermal heat exchanger was investigated [21]. Also, the effect of CuO/Water nanofluid in a heat exchanger was investigated and the results showed that the presence of nanofluid increases the discharge speed and thus improves the thermal efficiency [22]. The investigation of the two-phase nanofluid of Cu-water showed that under the condition of a w-shaper pipe 0.8% with volume fraction, the system performance maximizes [23]. The CFD method, the finite volume method is the widely used approach in order to discretize and solve the RANS equation [24,25].

This study investigates the effects of different parameters on the heat transfer performance of a CBHE system, which is located in a particular area of Iran (Sahand, East Azerbaijan) based on the CFD solution. The operating fluid inlet velocity, the groundwater seepage velocity, the soil porosity, and the use of nanofluids instead of pure water are studied. The novelty of this study is the utilization of the optimization method in order to attain maximum performance and find ideal operating conditions for the CBHE.

THEORETICAL SECTION
Problem description and Solution strategy

This type of BHE system can be installed in different areas that benefit from geothermal energy, as shown in Fig. 1; Iran has suitable areas for CBHE installation.

Therefore, Sahand region, located in East Azarbaijan province and has a temperature profile similar to the study of *Li et al.* [5] shown in Fig. 2, is considered a case study.

In the current study, based on the application of BHEs, a shallow CBHE is intended for domestic consumption. In this thermal cycle, cold water enters the CBHE. After receiving geothermal energy and increasing the temperature, it enters the heat pump. This heated water helps to heat a single-story building through the floor piping of the building. A schematic of a CBHE system in a building heating system is shown in Fig. 3.

The mechanism of the CBHE system is that cold water is sent from the space between two pipes into the ground and to a great depth. The inlet water temperature increases
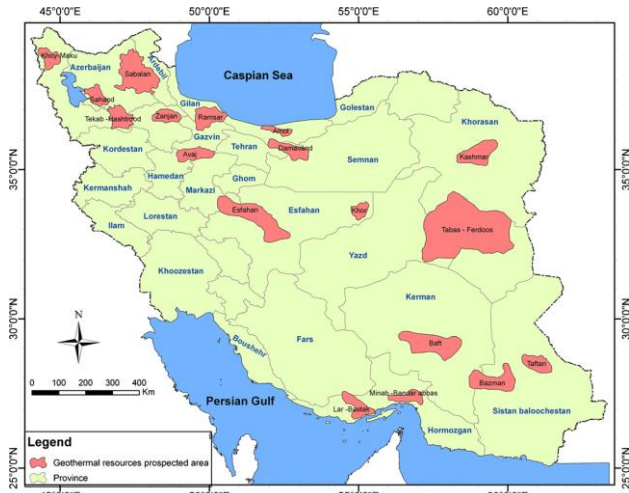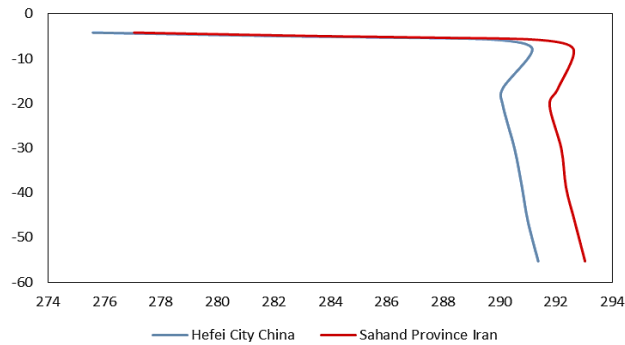
Fig. 1: Geothermal resources map of Iran [26]

Fig. 2: The ground temperature profile with depth [19,27]

Fig. 3: Schematic of a BHE installed in a single-story building thermal cycle
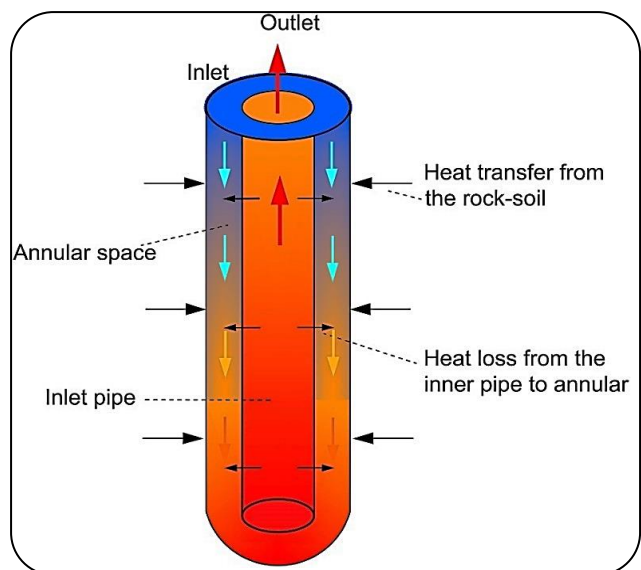
Fig. 4: Simple model of CBHE with its heat transfer mechanism geometry, dimensions, and properties.

due to its proximity to the soil and receiving thermal energy. Then, the heated water is pumped from the exterior space between the interior and exterior pipes to the ground surface. By changing the season, this process is reversed [28]. An example of a CBHE model is indicated in Fig. 4.

In this study, a rectangular cube with specific dimensions is considered the region's soil, then a borehole is drilled in the soil at a certain depth, and CBHE inside the borehole is assumed. Since the temperature of the soil layers is different from each other, which means that the soil temperature changes with increasing drilling depth, the rectangular cube has been divided into smaller pieces to model the temperature profile. The diameter and depth of the borehole are the same as the diameter and depth of the outer pipe. Thus, the outer tube is fixed inside it; therefore, the borehole is not drilled to the bottom of the soil, and the lower section remains intact. In this case, cement or polymer materials play the role of insulation for the outer pipe. The CBHE system consists of two coaxial tubes with specified thickness, diameter, and height.
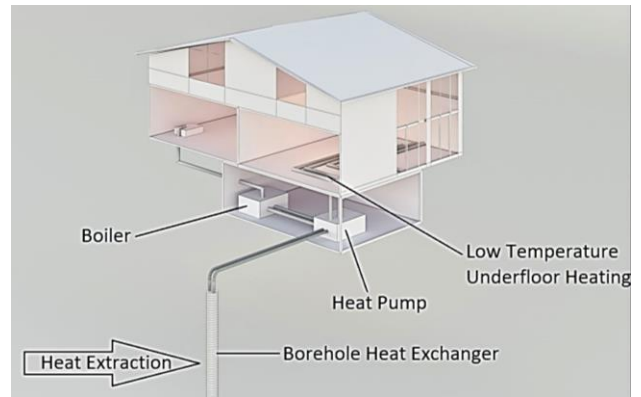
The outer pipe is the same length as the borehole, but the inner pipe is designed to be slightly shorter. The reason for this difference is during the creation of a gap between two pipes; from this gap, heated water is pumped to the ground surface. Here soil region is divided into eight parts; the first, seventh, and eighth layers are considered a kind of soil with no groundwater, and their properties are precisely like bedrock. The rest of the soil domain contains undrained porous soil with groundwater. It should be noted that the type of soil characteristics depends on the geological conditions of the region, and it can be different in each geographical area [29]. The geometry and dimension values of soil layers and pipes are shown in Fig. 5.

Tables 2 and 3 show the materials' thermal and physical properties used in the studied geometry. The physical and

Table 1: Geometrical parameters

Num.	Quantity	Value
1	Diameter of inner pipe	0.032(m)
2	Diameter of outer pipe	0.15(m)
3	Thickness of inner pipe	0.003(m)
4	Thickness of outer pipe	0.005(m)
5	Length of inner pipe	59.9(m)
6	Length of outer pipe	60(m)
7	Length of soil domain	65(m)
8	Width of soil domain	4(m)
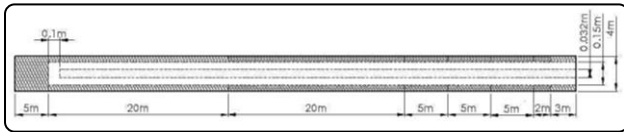
Fig. 5: Geometry and dimension values of different soil layers and pipes

thermal properties of the pipes have been considered based on the model studied by *Li et al.* [5]. Inner pipe material is regarded as Polyethylene (PE). Also, the physical and thermal properties of the soils in the geometry have been adapted from soil mechanics references [6,29]. In the present study, the ground space where the borehole and CBHE have been installed consists of two soil types. One type is undrained porous soil in which groundwater flows, and another type is impermeable soil or bedrock that is not considered a porous medium. Thus there is no water seepage in that region. Also, in this simulation, the presence of nanofluids as working fluid, instead of pure water, two different nanofluids are used, and the properties of which are given in Table 2 [20].

All dimensions Fig. 5 are shown in Table 1.

Fluid mechanic equations and turbulence flow equations

The (RANS) equations can be applied to analyze liquid flow in three dimensions. According to the RANS equation, the continuity, momentum, and energy equations are represented in equations 1 to 3 respectively [30]:

$$\frac{\partial \overline{u_i}}{\partial x_i} = 0 \tag{1}$$

$$\rho \left[\overline{u_j} \frac{\partial \overline{u_i}}{\partial x_j} \right] = -\frac{\partial \overline{P}}{\partial x_i} \left[\mu \left(\frac{\partial \overline{u_i}}{\partial \overline{x_j}} \right) - \rho \overline{u_i' u_j'} \right] \tag{2}$$

$$\rho c_p \overline{u_j} \frac{\partial \overline{T}}{\partial x_j} = \frac{\partial}{\partial x_j} \left[\lambda \left(\frac{\partial \overline{T}}{\partial \overline{x_j}} \right) - \rho \overline{u_j' T'} \right] \tag{3}$$

Table 2: Thermal and physical properties of liquid materials

Num.	Quantity	Value
1	Density of water	998.2(kg/m3)
2	Specific heat of water	4182(J/kg.K)
3	Thermal conductivity of water	0.6(W/m.K)
4	Density of Al_2O_3	3790(kg/m3)
5	Specific heat of Al_2O_3	765(J/kg.K)
6	Thermal conductivity of Al_2O_3	40(W/m.K)
7	Density of CuO	6320(kg/m^3)
8	Specific heat of CuO	532(J/kg.K)
9	Thermal conductivity of CuO	76(W/m.K)

Table 3: Thermal and physical properties of solid materials

Num.	Quantity	Value
1	Density of inner pipe	960(kg/m^3)
2	Specific heat of inner pipe	2300(J/kg.K)
3	Thermal conductivity of inner pipe	0.43(W/m.K)
4	Density of outer pipe	8300(kg/m^3)
5	Specific heat of outer pipe	2300(J/kg.K)
6	Thermal conductivity of outer pipe	16.37(W/m.K)
7	Density of undrained porous soil	2251.41(kg/m^3)
8	Specific heat of undrained porous soil	640.1(J/kg.K)
9	Thermal conductivity of undrained porous soil	2.738(W/m.K)
10	Density of bedrock	1650(kg/m^3)
11	Specific heat of bedrock	1048(J/kg.K)
12	Thermal conductivity of bedrock	1.992(W/m.K)
13	Soil porosity	0.44
14	Density of grout	1860(kg/m^3)
15	Specific heat of grout	1200(J/kg.K)
16	Thermal conductivity of grout	1.6(W/m.K)
17	Density of limestone	2000(kg/m^3)
18	Specific heat of limestone	1465(J/kg.K)
19	Thermal conductivity of limestone	3.3(W/m.K)

Where *u* is the velocity (m/s) component, *x* is the direction (m) component, and P is pressure (Pa).

The energy relation of the rigid sides which contain the inside and outside of the pipe walls is [30]:

$$\nabla(\lambda_S \nabla T_S) = 0 \tag{4}$$

Since the length of the pipe is very long, the Reynolds number is more significant than 2000, so turbulent flow is considered for the operating fluid. The RNG k-ε model is assumed for turbulent flow modeling for proper flow prediction at a distance from a wall with a relatively small
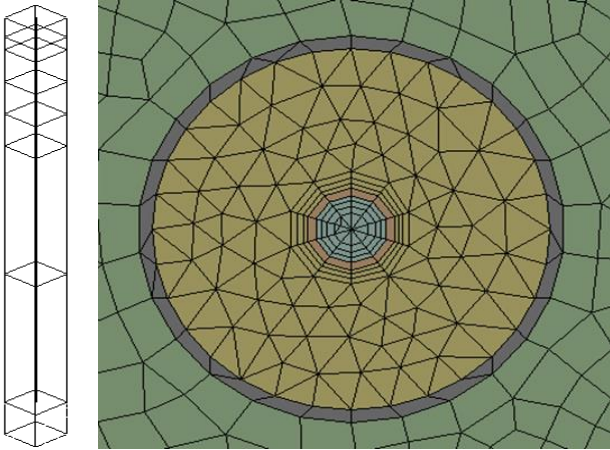
Fig. 6: Drawn geometry and meshing around the inner and outer pipe

pressure gradient. Also, RNG k-ε features make this model more accurate and reliable for different conditions. This turbulence model has good performance in industrial applications and good accuracy. It is also stated that the k-ε model has better accuracy at low speeds than the k-ω model. This model uses an additional term in the ε transfer equation, which increases its accuracy in simulating turbulent flows with Rapidly Strained. The effect of flow rotation on turbulence viscosity is also considered a result. Simulation accuracy increase can be seen in simulating rotational flows. While the k-ε Standard model is suitable for high Reynolds, the RNG model offers an analytical solution-based differential relationship for effective viscosity in low Reynolds. The model provides more accurate answers for low Reynolds in the near wall domain and it offers benefits in complicated configurations since computational grid points are maintained by using the larger wall function and wall spacing on non-essential proportions of the geometry and integrating to the wall where high-quality skin friction or heat transfer is needed [31]. The equations of turbulent kinetic energy transport (k) and the rate of dissipation (ε) are as follows [31]:

$$\frac{\partial(\rho k \overline{u_j})}{\partial x_j} = \frac{\partial}{\partial x_j}\left[\left(\mu + \frac{\mu_t}{\sigma_k}\right)\frac{\partial k}{\partial x_j}\right] + G_k - \rho\varepsilon \tag{5}$$

$$\frac{\partial(\rho \varepsilon \overline{u_j})}{\partial x_j} = \frac{\partial}{\partial x_j}\left[\left(\mu + \frac{\mu_t}{\sigma_\varepsilon}\right)\frac{\partial \varepsilon}{\partial x_j}\right] + \frac{\varepsilon}{k}(C_{\varepsilon 1}G_k - C_{\varepsilon 2}\rho\varepsilon) \tag{6}$$

Where the dynamic viscosity is μ(kg/m.s), the converse Turbulence Prandtl number for k and ε is σ_k and σ_ε, and the amount of production for TKE according to the medial speed gradient is G_k.

Table 4: values and constants of RNG k-ε model [30]

C_μ	$C_{\varepsilon 1}$	$C_{\varepsilon 2}$	σ_k	σ_ε
0.0845	1.42	1.68	0.7194	0.7194

$$G_k = \mu_t\left(\frac{\partial u_i}{\partial x_i} + \frac{\partial u_i}{\partial x_j}\right)\frac{\partial \overline{u_i}}{\partial x_i} - \frac{2}{3}\rho k \delta_{ij}\frac{\partial \overline{u_i}}{\partial x_i} \tag{7}$$

$$\mu_t = C_\rho k^2 / \varepsilon \tag{8}$$

μ_t is turbulent viscosity. Other values and constants are given in Table 4.

Numerical modeling and simulation
Model design and meshing

For numerical analysis and simulation, the firstly chosen geometry is drawn, which, as mentioned before, includes eight soil layers, boreholes, and a CBHE in Ansys Design Modeler software, which can be seen in Fig. 6. Then meshing for the drawn geometry with Ansys Meshing software is done. The boundary layer mesh has also been used to precisely limit the solution and prevent a sudden increase in speed and temperature in the pipe walls. The meshing of the inner and outer pipes can be seen in Fig. 6.

The quality of meshing is determined based on two criteria, skewness, and orthogonal quality, which can be calculated in Ansys Fluent and the range of 0.5 to 0.8 and 0.2 to 0.7 are suitable for skewness and orthogonal quality [32]. In the above meshing, skewness and orthogonal quality values were evaluated at about 0.7 and 0.8 respectively, which had a suitable agreement with target values.

Boundary and operating conditions

After meshing, the prototype is entered into finite volume software for numerical analysis and simulation. Ansys Fluent software version 2019 has been selected for this numerical simulation. Then the boundary conditions and initial conditions for the model are defined. At the inlet of the CBHE pipe, the operating fluid is applied at a constant temperature and speed. Soil temperature profiles around CBHE are taken from the study of *Guichen Li et al.* [6]. At the interaction faces of the fluid and solid elements, these suppositions are obtained [6]:

$$\vec{u} = 0 \tag{9}$$

$$T = T_s \tag{10}$$

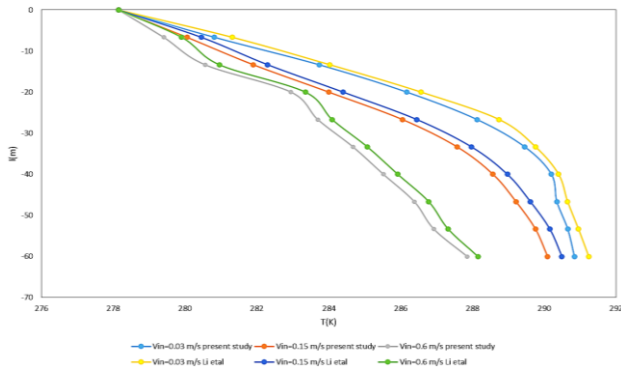$$-\lambda_s \frac{\partial T_s}{\partial n} = -\lambda_f \frac{\partial T}{\partial n} \tag{11}$$

Fig. 7: Comparison of the results of Guichen Li et al. [6] and the present study for operating fluid temperature changes at different velocities

Fig. 8: Fluid temperature at a depth of 60 meters inside the outer pipe in different meshes

Where λ_s is thermal conductivity (W/m.K) for the solid wall, λ_f is thermal conductivity (W/m.K) for the heat carrier fluid, T_s is the solid wall temperature (K), and n is the local coordinate vertical (m) to the solid wall. It should be noted that the turbulence intensity is considered to be 5%.The soil temperature changes with increasing depth. The variation of the temperature profile can be determined from this relation [6]:

$$T_s(x,\tau) = T_m + A_m\, exp\left(-\sqrt{\frac{\omega}{2\alpha_s}}x\right) cos\left(\omega\tau - \sqrt{\frac{\omega}{2\alpha_s}}x\right) \tag{12}$$

Here x(m) is called the ground depth, which is obtained from the top plane, τ (hour) is considered as the time when the annual fluctuation of the top plane temperature occurs, $T_s(x,\tau)$ is the ground temperature when x is the depth and the time is τ; A_m (°C) is considered as the annually frequent fluctuation for the top plane, ω is used for the annual frequency of the temperature, T is the annual duration of the temperature, α_s (m²/s) is the geothermal conductivity coefficient. T and ω are calculated as follows [6]:

$$\omega = \frac{2\pi}{T = 0.00071725} \tag{13}$$

$$T = 8760h \tag{14}$$

An essential point in this study is the existence of groundwater seepage. For this purpose, groundwater from the second to seventh layers in the -x direction enters the soil space at a constant speed and temperature, and after passing through the borehole and CBHE well, it leaves the other side of the soil. The pipe outlet and the soil outlet domain are pressure outlet conditions. It should be noted that the amount of porosity should be defined in the layers
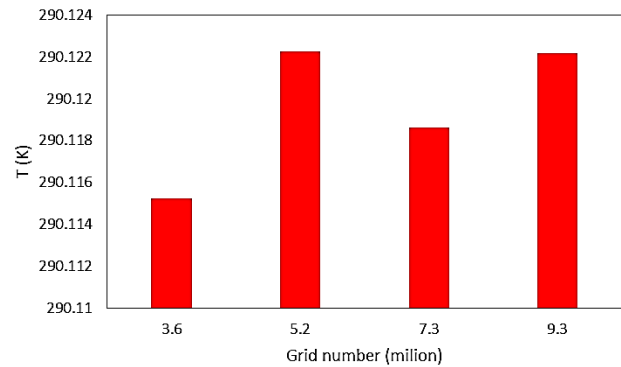
of soil where water seepage is considered. Naturally, groundwater flow has a small Reynolds number due to its shallow velocity, which is regarded as a laminar flow.

Validation and grid independence

In the first step of a numerical simulation, it is necessary to validate the numerical model with a sample. The model used in *Guichen Li et al.* [6] is selected. This model includes a CBHE that is assumed to have a variable temperature profile on the outer wall surface of the outer pipe. This temperature profile is calculated by Eq. (12). In this simulation, groundwater seepage flow and porous zone are not considered for the soil, and only the effect of soil temperature changes with increasing depth is considered. For this validation, cold water with a constant temperature of 278.15 K is entered into the inlet pipe. According to the main study, three different speeds 0.03 m/s, 0.15 m/s, and 0.6 m/s were studied. The comparison results are shown in Fig. 7. The maximum error between present study results and experimental results was about 0.5%. The results obtained from the numerical simulation with the original sample showed acceptable agreement, so it can be claimed that the developed model has good accuracy.

In the next step, a mesh independence solution was performed. Mesh around the pipes and water domain generated properly to observe water temperature changes. To check grid independence, three different meshes were generated. It should be noted that the geometry was examined for 3.6, 5.2, and 7.3 million elements, and the temperature at the end of the inner pipe at a speed of 0.15 m/s was calculated for three cases. The results are shown in Fig. 8.

As shown in Fig. 8, the temperature value of the operating fluid at the end of the outer pipe at a depth of

60 meters in the number of different meshes shows almost the same values. However, due to varying both the y+ value and wall mesh sizing the fluid temperature value has varied slightly. As a result, the grid independence shows acceptable results. y+ makes dimensionless the vertical distance between the center of the mesh elements and the wall. This parameter is used to evaluate the appropriateness of the grid element size (height) around the pipe wall boundaries and its value is calculated by following equations [30].

$$y^+ = \frac{yu_\tau}{\nu} \tag{15}$$

$$u_\tau = \sqrt{\frac{\tau_w}{\rho}} \tag{16}$$

$$\tau_w = \frac{1}{2} C_f \rho U_\infty \tag{17}$$

$$C_f = 0.079 \, Re^{-0.25} \tag{18}$$

In the above equations, *y* is the vertical distance from the grid element center to the wall boundary, u_τ is frictional speed, τ_w is wall shear stress, U_∞ is the free stream velocity, and C_f is the wall friction factor. In this simulation, the enhanced wall treatment was utilized for proper flow prediction near walls. Therefore, 7 inflation layers with Y^+ of near 5 are generated which is suitable for low Reynolds number flows.

Performance evaluation method

Different parameters affect the thermal efficiency of CBHE. In this study, the effect of various parameters such as inlet water velocity in the pipe, the presence of groundwater seepage at different velocities, the amount of varying porosity for the soil around CBHE, and the company of nanofluids and their application instead of water-carrying fluid have been given special attention. Each of these is solved separately and numerically simulated.

Heat career of CBHE

The heat career indicates the heat transfer of the working fluid between the interior pipe and the exterior pipe and the heat transfer between the water inside the pipe and the ground. The thermal efficiency of CBHE can be calculated by determining the heat career distribution and temperature changes. The temperature of the working fluid in the free space rises upside-down; also, as the operating fluid in the interior pipe rises and

moves towards the ground, the temperature of the fluid changes. As a result, heat acquired from the soil domain for CBHE is achieved by flowing in gaps. That can be given in the following equations [33]:

$$Q_{bottom} = C_w V_{in}(T_{bottom} - T_{in}) \tag{19}$$

The actual heat extraction can be defined as the following equation:

$$Q_{act} = C_w V_{in}(T_{out} - T_{in}) \tag{20}$$

Where *C* is the Specific heat capacity (J/kg.K) and *Q* is assumed as heat load (kW). The thermal drop ratio due to the operating fluid along the inside pipe and the gaps are defined by the following equation.

$$\beta = \frac{Q_{bottom} - Q_{act}}{Q_{bottom}} = \frac{T_{bottom} - T_{out}}{T_{bottom} - T_{in}} \tag{21}$$

It should be noted that since the radius for the system pipes is not very large compared to the surrounding soil, just the temperature changes of the operating fluid inside the pipe along the depth of the pipe (i.e., direction z) were considered and the void fraction of air and the fluid was not considered and the pipes only contained the water [34].

Groundwater velocity

Heat transfer due to CBHE and the soil domain is influenced by various parameters such as physical and thermal properties of the working fluid inside the pipes, flow conditions such as velocity and turbulence, physical and thermal properties of soil, soil porosity, velocity, and groundwater properties, etc. A noteworthy point in the simulation is that the ground is a homogeneous porous medium, and its mass force, the effect of heat radiation, and its loss of viscosity are ignored. Obviously, mentioned effects can affect the results which cause differences with the natural conditions [34]. By assuming a porous environment with θ porosity, volumetric heat capacity C_p (J/kg.K), thermal conductivity coefficient λ_p (W/m.K), thermal diffusivity α_p (m²/s) can be calculated as follows [35]:

$$C_m = \theta C_w + (1 - \theta)C_s \tag{22}$$

$$\lambda_m = \theta \lambda_w + (1 - \theta)\lambda_s \tag{23}$$

$$\alpha_m = \frac{\lambda_m}{C_m} \tag{24}$$

Groundwater velocity is calculated from the Darcy equation [29]:

$$V_g = -k\nabla H \tag{25}$$

Where k is the permeability factor calculated by bellow equation:

$$k = \frac{QL}{hAt} \tag{26}$$

Where Q is the discharge flow rate of groundwater velocity (m^3/h), L is the width of soil region (m), t is the time that the groundwater passes the soil (s), A is the area of seepage surface (m^2), and h is the vertical height of groundwater path (m) which because of the small slope degree of soil could be ignored [29]. If a hydraulic gradient is assumed to be perpendicular to the CBHE pipes inside the undrained porous soil layers and v_g is the Darcy velocity (m/d), the first equation in the soil heat transfer problem is written as follows [35]:

$$C_p \frac{\partial T}{\partial t} + C_w V_g \frac{\partial T}{\partial x} = \nabla \cdot (\lambda_p \nabla T) \tag{27}$$

According to Eq. (28), the thermal response and temperature changes in the porous medium are defined as follows [35]:

$$T(x,y,t) = T_{g0} + \frac{q}{4\pi\lambda_p} exp\left(\frac{U_g}{2\alpha_p}\right) \int_0^{r^2/(4\alpha_p t)} \frac{1}{\psi} exp\left(-\frac{1}{\psi} - \frac{U^2 r^2 \psi}{16\alpha^2_p}\right) d\psi \tag{28}$$

Where U_g (m/s) indicates the effective velocity of groundwater following:

$$U_g = V_g \frac{C_w}{C_p} \tag{29}$$

As the time approaches infinity, a steady-state solution appears; the equation of that is as follows:

$$T_s(x,y) = T_{g0} + \frac{q}{2\pi\lambda_p} exp\left(\frac{U_g}{2\alpha_p}\right) K_0\left(\frac{U\sqrt{x^2+y^2}}{2\alpha_p}\right) \tag{30}$$

Where K_0 is the modified Bessel function of the second type of order zero. In certain conditions where the Darcy velocity is null, the thermal response and temperature changes are as follows:

$$T(x,y,t) = T_{g0} + \frac{q}{4\pi\lambda_p} Ei\left(-\frac{x^2+y^2}{4\alpha_p t}\right) \tag{31}$$

where E_i is the exponential integral function

Soil Porosity and backfill

According to the geometry, groundwater flows from the beginning of the second layer to the seventh layer. Also, the equations related to groundwater flow, which include the relationship between Darcy velocity and heat transfer equations, are given in full. Therefore, it should be noted that groundwater flows in an undrained porous soil; thus, in these areas, a porous medium is assumed. This porous medium and

the percent porosity will effectively heat transfer. It is also possible to fill the surrounding around CBHE with different materials and use them as a thermal insulators. These materials can have porosity such as gravel or other types of soil or materials such as cement and grout that are not considered a porous medium and saturated soil. As a result, no groundwater flows through them. These materials can play the role of insulation and thus reduce the heat exchange between the system and the surrounding soil. The effect of these materials on the heat exchange of CBHE and the surrounding soil depends on their thermal and physical properties [36]. Heat transfer occurs in impermeable soils by solid soil particles and in undrained saturated soils advection through moving liquid water and also the solid particles of soil. Although hidden heat transfer occurs by phase-changing (e.g., freezing or evaporation) could happen in the surrounding soil. Also, it assumed that the soil and backfill remain homogeneous with constant properties along the heat exchanger. Still, these changes are supposed to be ignored for simplification and more straightforward simulation[37]. The thermal resistance of the borehole and the environment soil can be calculated by (TRT) or analytical methods. If the CBHE pipes are placed inside the borehole with a certain length and radius, the borehole thermal resistance is considered as a group of thermal resistors. Which are defined as follows [37,38]:

$$R_{total} = R_f + R_s + R_{grout} \tag{32}$$

$$R_f = \frac{1}{2\pi r_i h} \tag{33}$$

$$R_s = \frac{1}{2\pi\lambda_s} ln\left(\frac{r_o}{r_i}\right) \tag{34}$$

$$R_{grout} = \frac{1}{2\pi\lambda_{grout}} ln\left(\frac{r_b}{r_o}\right) \tag{35}$$

$$h = C_o Re^Y Pr^{0.35} \frac{\lambda_f}{r_i} \tag{36}$$

In the above equations, R_{total} (m.K/W) is the overall thermal resistance or the thermal resistance for surrounding soil. R_f (m.K/W) is the thermal resistance of the working fluid, R_s (m.K/W) is the heat resistance of the solid wall of the pipe, and R_{grout} (m.K/W) is the thermal resistance of the grout or backfill. Also, r_o and r_i are the radius of the inner and outer pipes. Finally, h is the convective heat transfer coefficient of the operating fluid, which is determined using the Reynolds and Prandtl numbers. In this equation, experimental correction

coefficients were used to increase the accuracy in calculating h, given in the following equations [37,38]:

$$Y = 1.013e^{-0.067a} \tag{37}$$

$$C_o = \frac{0.003a^{1.86}}{0.063a^3 - 0.674a^2 + 2.225a - 1.157} \tag{38}$$

In the above equations, a is equivalent to the outer diameter ratio to the inner diameter and is called the annular diameter ratio.

$$a = \frac{D_{out}}{D_{in}} \tag{39}$$

The surrounding soil domain is assumed cylindrical rather than a cube with a diameter equal to the cube side. It should also be noted that due to the large computational domain of the soil, its geometry does not significantly affect the results, and it can be claimed that this area is considered a far field.

Nanofluids

The presence of nanofluids is assumed instead of pure water as the operating fluid in heat exchangers. Dispersed nanoparticles create Brownian motions that increase the interaction and collision between the liquid and the particles, thus increasing the heat transfer rate and improving the heat exchanger's efficiency [19]. Also in CFD simulations, there are Reynolds stresses and turbulent heat flux caused by velocity and temperature fluctuations which should be simulated. According to Reynolds number and pipe geometry, U-RANs equations can suggest different turbulence models that can model turbulent heat transfer around the walls and areas away from the walls [39]. Nanofluids are prepared by dispersing nanoparticles in the base liquid. Proper dispersion is a primary condition for nanofluid performance. Nanofluid stability is also another leading challenge for researchers [19]. It should be clear that the homogeneous single-phase model has been used for the simulation. The reason for this choice is the small size of nanofluid particles. In the case of small nanofluid particles, this method gives accurate and appropriate answers [40].

Several parameters are considered to simulate the nanofluid flow inside the pipe, and there is a need to solve the equations of continuity, momentum, and energy. Also, to simplify the problem, assumptions are needed, which are [41]:

• Three-dimensional flow field

• Incompressible flow

• Using Boussinesq approximation for buoyancy force

• Consider dynamic viscosity and thermal conductivity loss as a function of temperature

According to the above suppositions, the equations of continuity, momentum, and energy are written as [41]:

$$\frac{\partial u_i}{\partial x_i} = 0 \tag{40}$$

$$\rho_{nf} = \left(\frac{Du_i}{Dt}\right) = -\frac{\partial P}{\partial x_i} + \mu_{nf}\frac{\partial^2 u_i}{\partial x_j \partial x_j} \tag{41}$$

$$\rho_{nf}C_{p,nf} = \left(\frac{DT}{Dt}\right) = \frac{\partial}{\partial x_i} + \left(\mu_{nf}\frac{\partial T}{\partial x_i}\right) \tag{42}$$

In the above equations:

$$\left(\frac{D}{Dt}\right) = \left(\frac{\partial}{\partial t} + u_j\frac{\partial}{\partial x_j}\right) \tag{43}$$

Since there is no phase change between the nanofluid and solid nanoparticles, the nanofluid specific heat and density are determined by using the theory of suspensions as the effect of each phase by the volume fraction of that phase which is represented below [42].

$$\rho_{nf} = (1 - \varphi)\rho_{bf} + \varphi\rho_p \tag{44}$$

$$\left(\rho C_p\right)_{nf} = (1 - \varphi)\left(\rho C_p\right)_{bf} + \varphi\left(\rho C_p\right)_p \tag{45}$$

The Hamilton Crosser model can obtain the thermal conductivity of Al$_2$O$_3$/Water nanofluids and CuO/Water nanofluids between the volume fraction range of 3% to 9%. This simple model, which considers only the thermal conductivity of particles and their volume fraction, cannot model the thermal conductivity at high temperatures. Also, the dependency of the nanofluid thermal conductivity on the temperature was not modeled. This model is given below [42].

$$\frac{\lambda_{nf}}{\lambda_{bf}} = \frac{\lambda_p + 2\lambda_{bf} - 2\varphi(\lambda_{bf} - \lambda_p)}{\lambda_p + 2\lambda_{bf} + \varphi(\lambda_{bf} - \lambda_p)} \tag{46}$$

Where λ (W/m.K) is thermal conductivity and φ is volume fraction. Another effective parameter in the single-phase flow model is the dynamic viscosity, which varies for different nanofluids, depending on the fluid material and the volume fraction of the available nanoparticles. Other equations for dynamic viscosity are obtained based on experimental results. For example, the Maiga equation gives the dynamic viscosity of Al$_2$O$_3$/Water nanoparticles with a volume fraction range of 2% to 10%[43]:

$$\mu_{nf} = \mu_{bf}(123\varphi^2 + 7.3\varphi + 1) \tag{47}$$

The Brinkman experimental equation is also presented to determine the dynamic viscosity of the CuO/Water

      Research Article

Table 5: Initial and boundary conditions

Num.	Quantity	Value
1	Operating fluid inlet velocities	0.03,0.15,0.6(m/s)
2	Inlet operating fluid temperature	278.15(K)
3	Groundwater velocity	5(m/d)
4	Groundwater temperature	288.15(K)
5	Porosity of saturated soil	0.44

Fig. 9: Changes in operating fluid temperature along the outside pipe.

nanofluid which is more accurate in low-volume fractions in the following [44]:

$$\mu_{nf} = \frac{\mu_{bf}}{(1-\varphi)^{2.5}} \tag{48}$$

RESULTS AND DISCUSSION
Effect of inlet water flow velocity

During this section, the effect of the inlet water velocity on the outer CBHE pipe was investigated. The working fluid was sent into the pipe at three different speeds in this simulation. It happens when groundwater flows at a constant rate into the saturated soil from the beginning of the second layer to the beginning of the seventh layer. The assumed values for the initial and boundary conditions are given in Table 5.

After applying the boundary conditions and software settings for three different speeds for the inlet water flow of the outer pipe, a simulation was performed, and the temperature changes of the operating fluid temperature during 60m were investigated. The results obtained for the temperature changes along the outer pipe in the presence of groundwater compared to the case where there is no groundwater can be seen in Fig. 9.

As shown in Fig. 9, temperature changes decrease with the increasing velocity of the working fluid inside the outer pipe. This fact indicates that as the velocity increases, the fluid passes the pipe faster and has less time to receive thermal energy. As the velocity increases, the temperature changes along the pipe. The fluid gets less thermal energy, and the system's efficiency is significantly reduced. As a result, in designing the CBHE system, an attempt is made to keep the inlet velocity of the pipes low to maximize the heat exchange between the operating fluid and the geothermal energy. Also, *Bidarmaghz et al*. achieved similar results which indicated that higher carrier fluid flow increased the efficiency of the CBHE [45]. Another result seen in Fig. 9 is the effect of groundwater velocity on the temperature changes of the working fluid inside the pipe. It is known
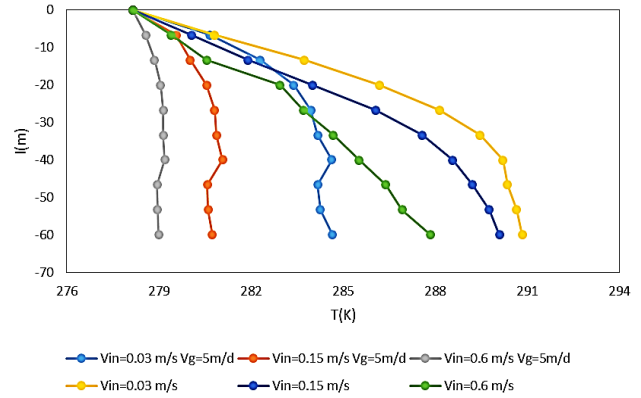
that when groundwater flow is considered in modeling, it has significant effects on heat transfer between the operating fluid and geothermal energy. The effects of groundwater flow are inevitable, and for the design of geothermal heat exchangers, drops due to water seepage must be predicted. This heat loss is due to water seepage can be reduced by placing insulating and non-porous layers in the borehole space that do not pass water flow. Thermal drops due to groundwater seepage are more visible at high velocities inside the pipe because the high velocity of the operating fluid reduces the fluid's temperature changes along the pipe; naturally, the seepage of groundwater worsens the situation and further reduces the temperature changes along the pipe. Therefore, the efficiency is significantly reduced. The velocity of the inlet working fluid has a significant effect on the pressure drop inside the pipe and as a result the CBHE efficiency. The pressure drop inside the pipe is calculated from the Darcy-Weissbach equation represented below [46].

$$\Delta P_l = \frac{F}{D} \frac{\rho V_{in}^{\,2}}{2} \tag{49}$$

$$F = \frac{0.3164}{Re^{0.25}} \tag{50}$$

$$\Delta P = \Delta P_l \times L \tag{51}$$

In the above equations, ΔP is pressure drop, F is friction coefficient and Re is Reynolds number which is equal to 1.8×10^6, 9×10^6 and 25×10^6 for inlet velocity of 0.03 (m/s), 0.15 (m/s), and 0.6 (m/s) respectively.

Fig. 10 shows the data about pressure drop and Reynolds number as a function of mass flow rate. Regarding the details, when is the flow rate, for the working
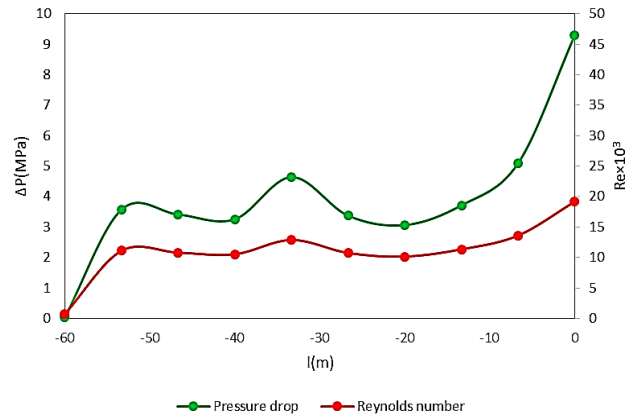
Table 6: Variations of the pressure drop and the Reynolds number along the pipe.

Num.	L (m)	V_{in}=0.6 (m/s)		V_{in}=0.15 (m/s)		V_{in}=0.03 (m/s)	
		Re	ΔP (MPa)	Re	ΔP (MPa)	Re	ΔP (MPa)
1	0	19169.33	9.291	4792.33	0.821	958.47	0.052
2	-6.67	13604.53	5.092	3410.27	0.457	679.93	0.027
3	-13.33	11347.77	3.713	2852.62	0.334	575.84	0.021
4	-20.00	10151.38	3.064	2551.07	0.272	508.43	0.0162
5	-26.66	10744.28	3.372	2701.48	0.301	535.78	0.0178
6	-33.33	12884.56	4.641	3232.58	0.412	639.00	0.024
7	-40.00	10524.77	3.253	2639.64	0.293	518.97	0.017
8	-46.66	10802.71	3.412	2715.09	0.301	538.18	0.018
9	-53.32	11092.20	3.571	2787.59	0.324	558.81	0.019
10	-60.00	697.59	0.031	169.37	0.011	34.78	0.001
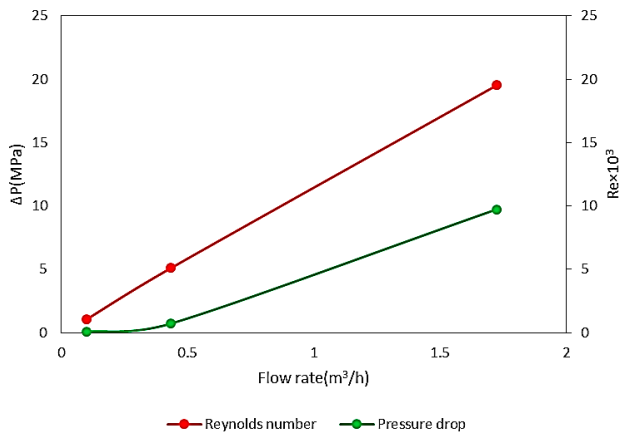
Fig. 10: Variations of the pressure drop and the Reynolds number with the flow rate.

the fluid velocity of 0.03 (m/s), 0.15 (m/s), and 0.6 (m/s) are equal to 0.09 (m³/h) 0.43 (m³/h) and 1.74 (m³/h) respectively, increased, Reynolds number and pressure drop along pipe grew which means that growing in unfavorable pressure drop led to a decline in temperature raise along CBHE pipe. To clarify the pressure and flow field along the whole computational domain, pressure drop and Reynolds number changes along the pipe is calculated. The results are shown in Table 6.

Regarding the data of Table 5 Reynolds number and Pressure drop declined along the pipe which means at the end of the CBHE pipe, which had the lowest pressure drop, the highest temperature was achieved. Also as inlet velocity decreased the value of pressure dropped and the Reynolds number dropped steadily which means the lowest inlet velocity helped CBHE to obtain a better

Fig. 11: Variations of the pressure drop and the Reynolds number along the pipe.
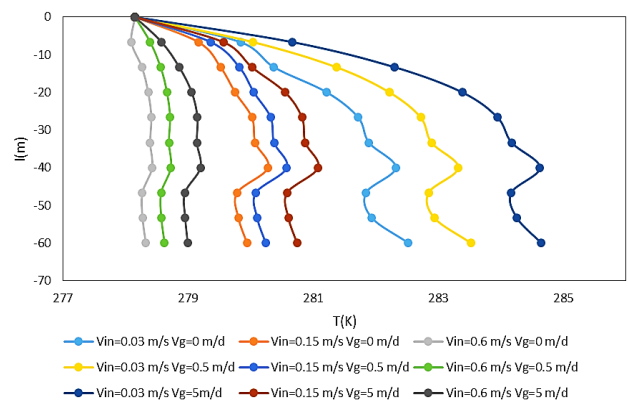
Fig. 12: Changes in operating fluid temperature along the outside pipe considering different groundwater velocities.

performance. As the variations of Reynolds number and pressure drop at V_{in}=0.6(m/s) was more remarkable than other conditions, the results of pressure drop and Reynolds number changes are illustrated in Fig. 11.

Looking at the details of Fig. 11 Reynolds number and pressure drop declined significantly along the CBHE pipe.

Effect of seepage velocity

In this section, in the first step, the temperature changes of the operating fluid inside the outer pipe along 60 meters in the presence of groundwater seepage at different speeds are evaluated and analyzed. Groundwater velocities of 0.5 m/d and 0 m/d will be evaluated rather than 5 m/d. The results of temperature changes of the working fluid along the outer pipe at different speeds and in the presence of groundwater seepage at various speeds are shown in Fig. 12. As can be seen from Fig. 12, and as expected, when the velocity of the operating fluid inside the pipe increased, the temperature changes along the outside pipe decreased.
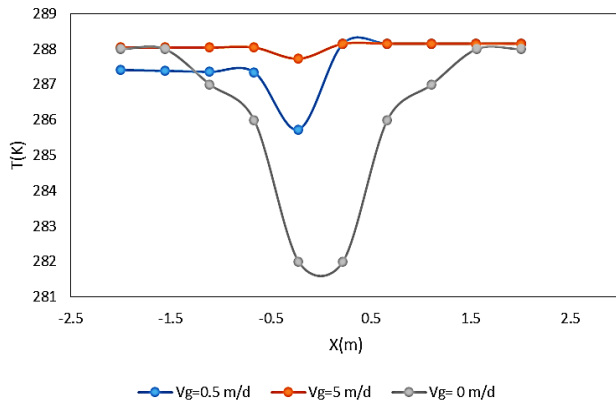
Research Article

Fig. 13: Groundwater temperature changes across soil width.

Fig. 14: Temperature changes of the operating fluid inside the pipe, taking into account different porosities.

The point that needs to be addressed in detail is the effect of different groundwater velocities on temperature changes inside the outer pipe. As the groundwater velocity decreases, it causes the operating fluid's temperature to change inside the outer pipe. The lower the groundwater seepage rate, the longer the groundwater is around the pipe. As a result of this proximity, the heat transfer rate between the operating fluid and the ground heating source decreases, and the water inside the pipe heats up less. If the seepage rate is considered equal to 0 m/d, the groundwater permanently surrounds the outer pipe. Obviously, in these conditions, the rate of heat transfer and increase in temperature of the operating fluid is minimal. It should be noted again that these conditions are geotechnical properties of the region's soil and cannot be prevented, but as mentioned, placing insulating materials in the borehole can improve these conditions.

Another point that can be considered in this section is the changes in groundwater temperature. Regarding the operating fluid sample velocity of 0.15 m/s, groundwater temperature changes at three different velocities of 5 m/d, 0.5 m/d, and 0 m/d across the soil are investigated. Other conditions, including temperature and soil porosity, are obtained from Table 5 .The results are shown in Fig. 13.

As can be seen from the diagram in Fig. 13, when the rate of groundwater seepage across the soil is lower, and its temperature changes are more significant. This temperature drop is because the groundwater temperature is initially assumed to be higher than the working fluid temperature inside the pipe. Also, a similar study was conducted by *Zhang et.al* on the U-tube heat exchanger which concluded that ignoring the groundwater advection augments the heat transfer rate[47]. Due to its proximity
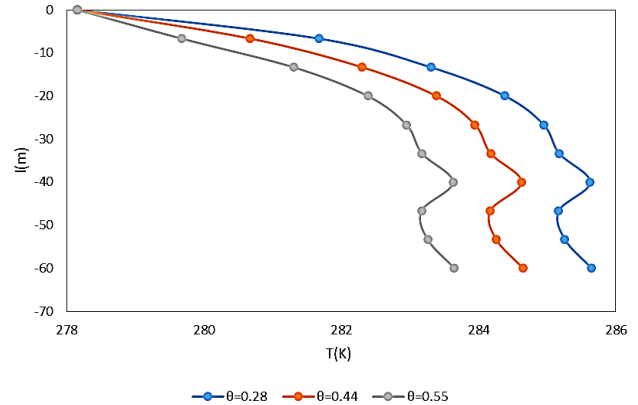
to groundwater, thermal energy is decreased, and its temperature drops. But after passing around the pipe, it receives heat from the ground again and reaches its initial temperature. This temperature drop is most extraordinary when the groundwater velocity is 0 m/d.

Effect of Soil Porosity and backfill

The main focus is on the soil porosity, and its effect on changes in water temperature inside the pipe and groundwater has been observed. To simulate, we consider the water velocity inside the pipe equal to 0.03 m/s and the groundwater velocity 5 m/d. The reason for considering the above values for this simulation is that the temperature changes at these speeds are more noticeable. The maximum changes in the temperature of the operating fluid inside the pipe and the changes in groundwater temperature occur at the mentioned speeds. Also, for the values of soil porosity around the pipe in which groundwater flows, two values of 0.28 0.55, and 0.44 are examined. These values are selected from geotechnical references [29]. Fig. 14 shows the temperature changes of the operating fluid inside the pipe in the presence of groundwater, taking into account different porosity values for the soil. It must be stated that the empty places of porous media area are filled by water. In other meaning, the porous media is 100% saturated with groundwater.

With increasing soil porosity, it is clear that the space between soil particles increases and this space is filled with groundwater. In this case, the pipe carrying the operating fluid will contact a larger volume of groundwater, thus increasing the heat exchange between the pipe wall and groundwater. Increasing the heat transfer rate between
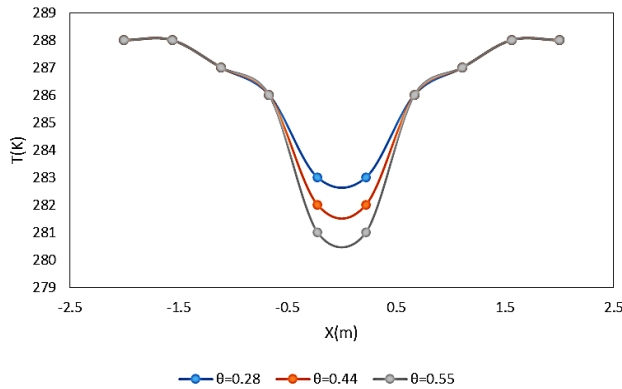
Fig. 15: Temperature changes of the groundwater taking into account different porosities.

Fig. 16: Temperature changes of the operating fluid inside the pipe, taking into account different porosities for backfill.

the pipe and groundwater reduces the temperature of the operating fluid along the length of the pipe. Therefore, as shown in Fig. 14, if the porosity is 0.55, the temperature increases along with the pipe decrease; on the other hand, increasing the volume of water accumulated in the porous soil around the pipe leads to an increase in thermal resistance and also an increase in temperature drop. As a result, the rise in temperature inside the pipe decreases, and system efficiency decreases. This fact indicates that before installing CBHE, the soil properties of the area should be checked to minimize soil porosity. Fig. 15 shows the changes in groundwater temperature across soil width under different values for the porous medium.

As mentioned in the previous section, with the increasing porosity of saturated soil, the available space for the placement of groundwater increases, and as can be seen from Fig. 14, in the case of increased porosity, changes in groundwater temperature have become more significant. This increase in temperature difference was due to more water among the soil particles. It is known that the thermal conductivity of water is lower than that of soil; in other words, it has more thermal resistance; therefore, with decreasing thermal conductivity, the rate of groundwater temperature drops increases. On the other hand, more groundwater is placed around the pipe, which causes a further decrease in groundwater temperature. It can also be claimed that by creating space between soil particles and the presence of water, the thermal resistance increases, and therefore the temperature drops decrease.

In this section, the effect of porosity on saturated soil was mentioned. It was determined that increasing soil porosity creating more gaps and the presence of water increases the thermal resistance. As a result, the operating
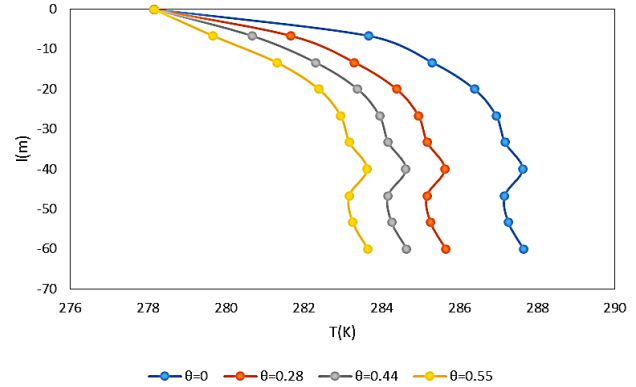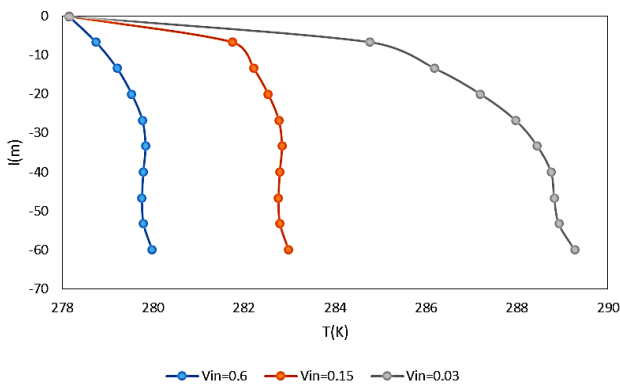
fluid temperature inside the pipe increases less. In general, it was found that groundwater inherently reduces the temperature difference of the working fluid inside the pipe. It is possible to reduce the rate of this temperature drop by digging a borehole around the CBHE system and filling it with various materials to improve the system's thermal performance. For this purpose, we consider the borehole inside the soil region once filled with undrained porous soil with a porosity of 0 examined, then the presence of saturated soil with porosity of 0, 0.28, 0.44, and 0.55 as backfill. The values of the operating fluid velocity and groundwater velocity are also considered as in the previous section. Also, the properties of undrained porous soil are given in Table 3. The results can be seen in Fig. 16.

Regarding Fig. 16, the soil porosity is considered to be 0, and the soil behavior is similar to bedrock in that there is no gap between the soil particles. Consequently, there is no seepage in this section. Therefore, with the absence of groundwater and increasing thermal conductivity, the thermal resistance in reaches its lowest value, and the temperature of the operating fluid rises. *Basok et. al* provided a similar conclusion which showed that greater heat extraction provides less soil porosity[48]. In other conditions where the backfill space is filled with soil similar to the area with the same porosity, no significant difference was observed. To show the impact of backfill thermal properties, cement, and limestone are considered as backfill. The thermal properties of grout and limestone can be seen in Table 3. The results are shown in Fig. 17.

As shown in Fig. 17, the operating fluid temperature along the pipe increased further with increasing thermal conductivity. As previously emphasized, with increasing thermal conductivity, the amount of heat resistance decreases,
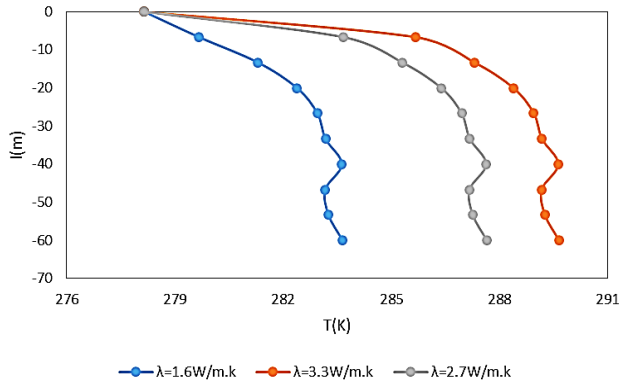
Fig. 17: Temperature changes of the operating fluid inside the pipe, taking into account different materials with different thermal conductivity for backfill
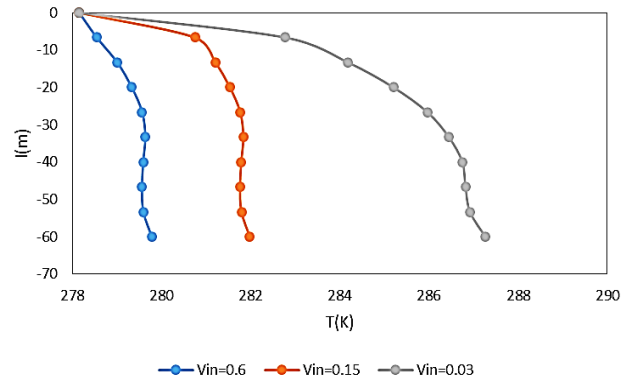

Fig. 19: Changes in operating fluid (Al₂O₃/water) temperature along the outside pipe considering inlet velocities

Fig. 18: Changes in operating fluid (CuO/water) temperature along the outside pipe considering different inlet velocities

Fig. 20: Changes in operating fluid temperature along the outside pipe considering different operating fluids.
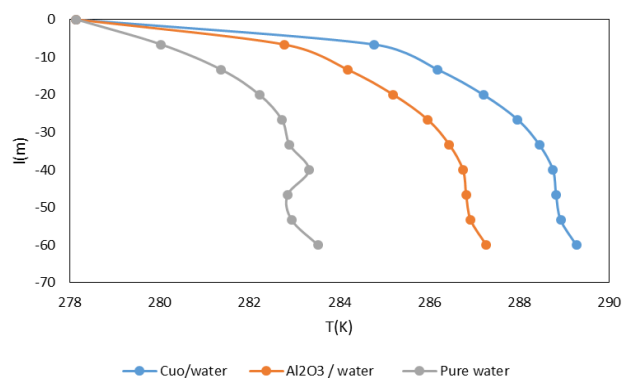
Effects of Nanofluids

This section discusses the effect of using a suitable nanofluid instead of pure water as the operating fluid in the CBHE system. Therefore, two nanofluids, Al_2O_3/Water and CuO/Water are selected to use as the operating fluid. The physical and thermal properties of nanofluids are given in Table 2. The effect of nanofluid inlet velocity on the rate of increase of working fluid temperature along the pipe is considered. Thus, three different velocities of 0.03 m/s, 0.15 m/s, and 0.6m/s are considered. It should be noted that the groundwater velocity is fixed and equal to 0.5 m/d. The results are shown in Fig. 18 and Fig. 19.

As shown in Fig.s 18 and 19, temperature changes along the pipe in the presence of nanofluids decrease with increasing inlet velocity, and their thermal behavior is precisely the same as water. As a result, it was observed

that like the water-operating fluid at the lowest inlet speed, the highest temperature increase is obtained along the pipe. Another vital issue to consider is the choice of operating fluid for the CBHE system. To achieve this aim, three types of fluids, pure water, Al_2O_3/water, and CuO/water, are analyzed at a specific rate of 0.03 m/s, where temperature changes along the pipe are more significant to measure. The results are shown in Fig. 20.

As shown in Fig. 20, operating fluid CuO/Water has the highest temperature change along the pipe and at a depth of sixty meters compared to the other two working fluids receiving the most heat from geothermal energy and increased temperature. This fact indicates that in the design of CBHE, it is better to use nanofluids instead of pure water because with the presence of nanofluids, the thermal conductivity of the operating fluid increases, followed by more fluid temperature. The study of the impact of utilizing nanofluids on the BHE done by *Diglio et al.* showed similar results which indicated that proper

Table 7: Goodness of Fit.

Model	Coefficient of etermination	Root Mean Square Error
Kriging	1	5.4758e-9
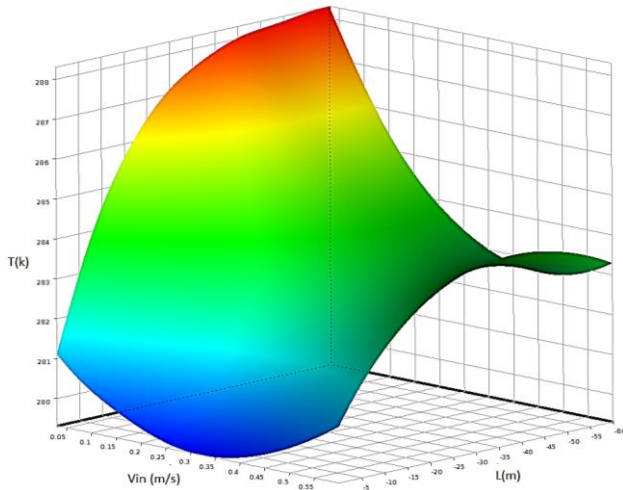
Fig. 21: Temperature changes along the outside pipe and different inlet velocities.
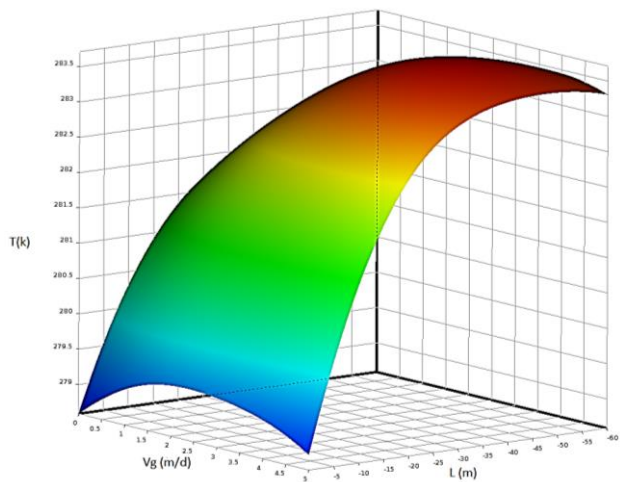
Fig. 22: Temperature changes along the outside pipe and different groundwater seepage velocities.

nanofluids can minimize borehole thermal resistance and improve efficiency. Finally, the thermal performance of the system is improved. Obviously, with the use of nanofluids with higher thermal conductivity, the rate of temperature increases.

Optimization

For the optimization process, the experiment needs to be designed. Since the investigation was pre-designed and the effect of different parameters was investigated,
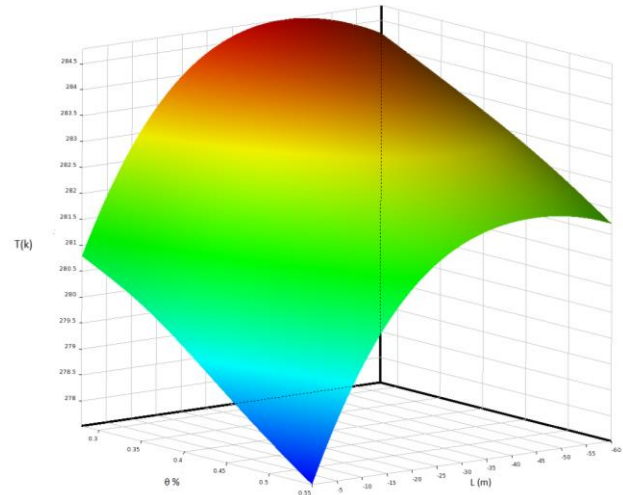
Fig. 23: Temperature changes along the outside pipe and different soil porosity.

the DOE method was set to custom mode. Following this, in the response surface section, different approaches were tried. According to the examination of the existing errors, the Kriging method with variable Kernel variation type was the best and most optimal mode. The Kriging method is a widely used and precise alternative model for response surface analysis. The relationship (response surface model) between the optimization objective (the highest value of power factor) and the design and operating parameters can be precisely defined based on the Kriging model [49,50]. The Kriging method parameters and goodness of fit are shown in Table 7.

All the effective parameters that were examined numerically are considered for the optimization process. However, since the CuO/water nanofluid has had the highest temperature growth in any different operating conditions, the impact of the type of operating fluid has been omitted. Subsequently, various diagrams were obtained based on the Kriging method, shown in Figs. 21 to 24.

According to the above diagrams, the highest temperature increase was illustrated at about 293 (k). The sensitivity coefficient of the parameters was obtained, which is shown in the pie chart below.

Looking at Fig. 25, the thermal conductivity of the backfill is the highest, and the porosity of the soil has the most negligible effect on the temperature increase along the outer pipe at 30.3% and 8.97%, respectively.

Finally, after the optimization process with the mentioned method, the optimal operating conditions were determined, given in Table 7.

**Table 7: Optimal operating conditions of The CBHE.**

Num.	Quantity	Value
1	Inlet water flow velocity	0.03 (m/s)
2	Groundwater seepage velocity	0.49 (m/d)
3	Soil porosity	0.28
4	Backfill thermal conductivity	3.3 (W/m.k)
5	Operating fluid	CuO/water
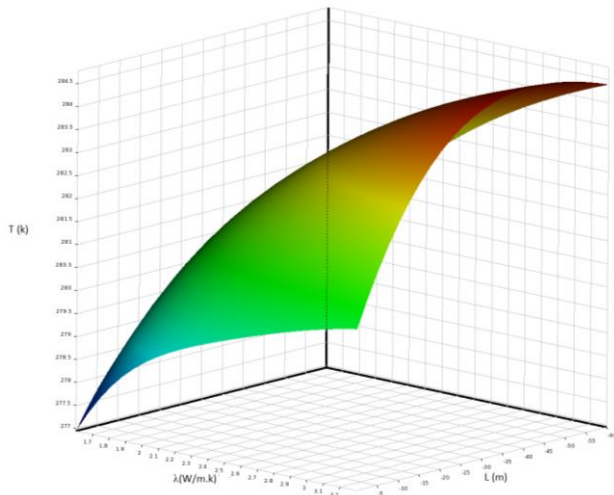
Fig. 24: Temperature changes along the outside pipe and different borehole thermal conductivity.

CONCLUSIONS

In this study, a special type of GSHP called CBHE was considered and effective parameters on the performance were studied. Parameters discussed in this study include operating fluid inlet velocity, groundwater velocity, soil porosity around the system, thermal insulation around CBHE, and the use of nanofluids instead of pure water. To simulate the effect of tangential velocity in CBHE pipes and groundwater seepage on the heat transfer and temperature rise along a 60-meter pipe, a 3-D modeling based on the CFD method is adopted. The study results on each case are briefly discussed in this section.

• As the inlet velocity of the working fluid increased, the temperature change along the pipe decreased due to less exposure time with geothermal energy. Therefore, the 0.03 m/s inlet velocity gave the highest temperature increase along the pipe.

• Three different seepage velocities of 0m/d, 0.5m/d, and 5m/d were examined. The lower the groundwater seepage velocity (0 m/d) caused, the more remarkable the fluid temperature drop inside the pipe.
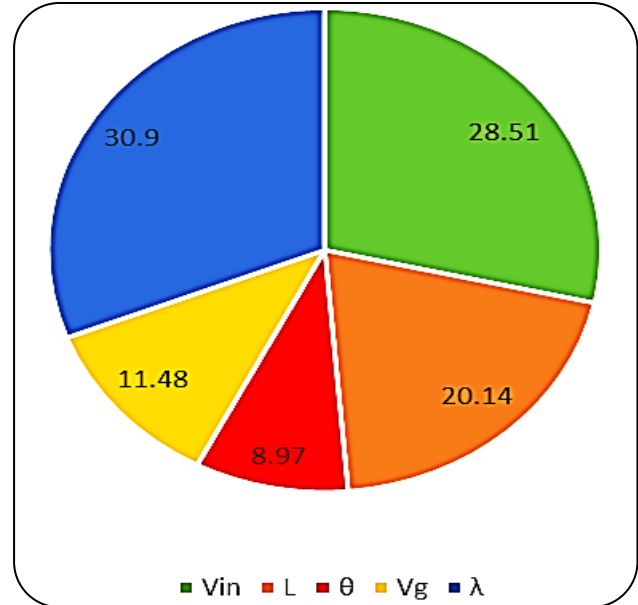
Fig. 25: Local sensitivity.

• Three different porosities, 0.44, 0.28, and 0.55, were assumed for the soil layers. The results showed that when the porosity is 0.55, the groundwater temperature has the most significant decrease. Also, it was shown that limestone with a thermal conductivity of 3.3 (W/m.K) causes the highest temperature increase of the operating fluid.

The presence of nanofluids Al_2O_3/water and CuO/water instead of pure water was considered and CuO/water attained better system performance due to its higher thermal conductivity. Also, the highest temperature augmentation occurred for both nanofluids at the lowest velocity (0.03m/s).

Nomenclature

Heat load at the bottom (kW)	Q_{bottom}
Actual heat load (kW)	Q_{act}
Water outlet temperature (K)	T_{out}
Water inlet temperature (K)	T_{in}
Water temperature at the bottom (K)	T_{bottom}
Water inlet velocity (m/s)	V_{in}
Darcy velocity (m/d)	V_g
Hydraulic head (m)	H
Specific heat capacity (J/kg.K)	C_p
Effective velocity (m/s)	U
Thermal resistance (m.K/W)	R
convective heat transfer coefficient of the circulating fluid (W/m².K)	h
Reynolds number of the circulating fluid	Re

Prandtl number	Pr
Heat loss ratio (%)	β
Porosity	θ
Thermal diffusivity (m²/s)	α
Thermal conductivity (W/m.K)	λ
Density (kg/m3)	ρ
Volume fraction (%)	φ
Dynamic viscosity (kg/m.s)	μ
Porous medium	m
Solid pipe wall	s
Water	w
Groundwater	g
Inner pipe	i
Outer pipe	o
Fluid	f
Borehole	b
Particle of nanofluid	p
Nanofluid	nf
Base fluid	bf
Coaxial borehole heat exchanger	CBHE
Ground source heat pump	GSHP
thermal response test	TRT
Reynolds averaged Naiver Stokes	RANS
Borehole heat exchanger	BHE
Turbulent kinetic energy	TKE
Re-Normalization Group	RNG

REFERENCES

[1] Li Y., Mao J., Geng S., Han X., Zhang H., Evaluation of Thermal Short-Circuiting and Influence on Thermal Response Test for Borehole Heat Exchanger, *Geothermics*, **50:** 136–147 (2014).

[2] Erol S., François B., Efficiency of Various Grouting Materials for Borehole Heat Exchangers, *Applied Thermal Engineering*, **70(1):** 788–799 (2014).

[3] Zhao J., Wang H., Li X., Dai C., Experimental Investigation and Theoretical Model of Heat Transfer of Saturated Soil around Coaxial Ground Coupled Heat Exchanger, *Applied Thermal Engineering*, **28(2–3):** 116–125 (2008).

[4] Beier R.A., Acuña J., Mogensen P., Palm B., Borehole Resistance and Vertical Temperature Profiles in Coaxial Borehole Heat Exchangers, *Applied Energy*, **102:** 665–675 (2013).

[5] Noorollahi Y., Pourarshad M., Jalilinasrabady S., Yousefi H., Numerical Simulation of Power Production from Abandoned Oil Wells in Ahwaz Oil Field in Southern Iran," *Geothermics*, **55:** 16–23 (2015).

[6] Li G., Yang J., Zhu X., Shen Z., Numerical Study on the Heat Transfer Performance of Coaxial Shallow Borehole Heat Exchanger, *Energy and Built Environment*, **2(4):** 445–455 (2021).

[7] Shoeibi H., Mehrpooya M., Assareh E., Izadi M., Pourfayaz F., Transient Simulation and Exergy Analysis of Heat-Pump Systems Integrated with Solar Compound Parabolic Collector, *Iranian Journal of Chemistry and Chemical Engineering (IJCCE)*, **41(6):** 2121–2134 (2022).

[8] Chen S., Mao J., Han X., Heat Transfer Analysis of a Vertical Ground Heat Exchanger Using Numerical Simulation and Multiple Regression Model, *Energy and Buildings*, **129:** 81–91 (2016).

[9] Abjadi A., Asadbeigi M., Farjyar S., Ghafoorian F., "3D CFD Investigation on Thermal Performance of a U-Tube Borehole Heat Exchanger", **11:** (2021).

[10] Li B., Han Z., Hu H., Bai C., Study on the Effect of Groundwater Flow on the Identification of Thermal Properties of Soils, *Renewable Energy*, **147:** 2688–2695 (2020).

[11] Ahmadi N., Ashrafi H., Rostami S., Vatankhah Reza, Investigation of the Effect of Gradual Change of the Inner Tube Geometrical Configuration on the Thermal Performance of the Double-Pipe Heat Exchanger, *Iranian Journal of Chemistry and Chemical Engineering (IJCCE)*, **42(7):** 2305-2317 (2023).

[12] Ma J., Jiang Q., Zhang Q., Xie Y., Wang Y., Yi F., Effect of Groundwater Forced Seepage on Heat Transfer Characteristics of Borehole Heat Exchangers, *Geotherm Energy*, **9(1):** 11 (2021).

[13] Jia G.S., Ma Z.D., Xia Z.H., Wang J.W., Zhang Y.P., Jin L.W., Investigation of the Horizontally-Butted Borehole Heat Exchanger based on a Semi-Analytical Method Considering Groundwater Seepage and Geothermal Gradient, *Renewable Energy*, **171:** 447–461 (2021).

[14] Jahangir M.H., Sarrafha H., Kasaeian A., Numerical Modeling of Energy Transfer in Underground Borehole Heat Exchanger within Unsaturated Soil, *Applied Thermal Engineering*, **132:** 697–707 (2018).

[15] Sheikholeslami M., Gerdroodbary M.B., Shafee A., Tlili I., Hybrid Nanoparticles Dispersion into Water Inside a Porous Wavy Tank Involving Magnetic Force, *J. Therm. Anal. Calorim.*, **141(5):** 1993–1999 (2020).

[16] Zhang C., Chen P., Liu Y., Sun S., Peng D., An Improved Evaluation Method for Thermal Performance of Borehole Heat Exchanger, *Renewable Energy*, **77:** 142–151 (2015).

[17] Zhu L., Chen S., Yang Y., Sun Y., Transient Heat Transfer Performance of a Vertical Double U-Tube Borehole Heat Exchanger under Different Operation Conditions, *Renewable Energy*, **131:** 494–505 (2019).

[18] Jarrahian A., Heidaryan E., A Novel Correlation Approach to Estimate Thermal Conductivity of Pure Carbon Dioxide in the Supercritical Region, *The Journal of Supercritical Fluids*, **64:** 39–45 (2012).

[19] Ali A.R.I., Salam B., A Review on Nanofluid: Preparation, Stability, Thermophysical Properties, Heat transfer Characteristics and Application, *SN Appl. Sci.*, **2(10):** 1636 (2020).

[20] Daneshipour M., Rafee R., Nanofluids as the Circuit Fluids of the Geothermal Borehole Heat Exchangers, *International Communications in Heat and Mass Transfer*, **81:** 34–41 (2017).

[21] Diglio G., Roselli C., Sasso M., Jawali Channabasappa U., Borehole Heat Exchanger with Nanofluids as Heat Carrier, *Geothermics*, **72:** 112–123 (2018).

[22] Sheikholeslami M., Haq R., Shafee A., Li Z., Elaraki Y.G., Tlili I., Heat Transfer Simulation of Heat Storage Unit with Nanoparticles and Fins through a Heat Exchanger, *International Journal of Heat and Mass Transfer*, **135:** 470–478 (2019).

[23] Zhou Y., *et al.*, A Two-Phase Simulation for Analyzing the Hydraulic-Thermal Performance of Cu–Water Nanofluid within a Tube Enhanced with W- and C-Shaped Ribs, *Case Studies in Thermal Engineering*, **43:** 102794 (2023).

[24] Samanipour H., Ahmadi N., Jabbary A., Effects of Applying Brand-New Designs on the Performance of PEM Fuel Cell and Water Flooding Phenomena, *Iranian Journal of Chemistry and Chemical Engineering (IJCCE)*, **41(2):** 618–634 (2022).

[25] Ashrafi H., pourmahmoud N., Mirzaee I., N. Ahmadi, Introducing a New Serpentine Configuration of Gas Channels to Enhance the Performance and Reduce the Water Flooding in the PEMFC, *Iranian Journal of Chemistry and Chemical Engineering (IJCCE)*, **42(1):** 192-207 (2022).

[26] Yousefi H., *et al.*, Developing the Geothermal Resources Map of Iran, *Geothermics*, **39(2):** 140–151 (2010).

[27] Yaria M., Javaani N., Ansari A., Moradian H., "Design and Installation of the First Geothermal Heat Pump in Iran" (2005).

[28] Fang L., Diao N., Shao Z., Zhu K., Fang Z., A Computationally Efficient Numerical Model for Heat Transfer Simulation of Deep Borehole Heat Exchangers, *Energy and Buildings*, **167:** 79–88 (2018).

[29] Das B.M., Das B.M., "Advanced Soil Mechanics", Taylor & Francis, New York, (2008).

[30] Nichols R.H., "Turbulence Models and their Application to Complex Flows", University of Alabama at Birmingham, Revision, UAB, (2010).

[31] Bejan A., Kraus A.D., Heat Transfer Handbook, John Wiley & Sons, (2003).

[32] Fatchurrohman N., Chia S.T., Performance of Hybrid nano-Micro Reinforced mg Metal Matrix Composites Brake Calliper: Simulation Approach, *IOP Conf. Ser.: Mater. Sci. Eng.*, **257:** 012060 (2017).

[33] Jiji L.M., Heat Convection, Springer Science & Business Media, (2009).

[34] Fan R., Jiang Y., Yao Y., Shiming D., Ma Z., A Study on the Performance of a Geothermal Heat Exchanger under Coupled Heat Conduction and Groundwater Advection, *Energy*, **32(11):** 2199–2209 (2007).

[35] Angelotti A., Alberti L., La Licata I., Antelmi M., Energy Performance and Thermal Impact of a Borehole Heat Exchanger in a Sandy Aquifer: Influence of the Groundwater Velocity, *Energy Conversion and Management*, **77:** 700–708 (2014).

[36] Choi W., Ooka R., Effect of Natural Convection on Thermal Response Test Conducted in Saturated Porous Formation: Comparison of gravel-Backfilled and Cement-Grouted Borehole Heat Exchangers, *Renewable Energy*, **96:** 891–903 (2016).

[37] Choi J.C., Park J., Lee S.R., Numerical Evaluation of the Effects of Groundwater Flow on Borehole Heat Exchanger Arrays, *Renew. Ene.*, **52:** 230–240 (2013).

[38] Dirker J., Meyer J.P., Convective Heat Transfer Coefficients in Concentric Annuli, *Heat Transfer Engineering*, **26(2):** 38–44 (2005).

[39] Menter F.R., Two-Equation Eddy-Viscosity Turbulence Models for Engineering Applications, *AIAA Journal*, 32(8): 1598–1605 (1994).

[40] Kim D., *et al.*, Convective Heat Transfer Characteristics of Nanofluids under Laminar and Turbulent Flow Conditions, *Current Applied Physics*, **9(2):** e119–e123 (2009).

[41] Sheikholeslami M., Ganji D.D., "Applications of Semi-Analytical Methods for Nanofluid Flow and Heat Transfer", Elsevier, (2018).

[42] Mintsa H.A., Roy G., Nguyen C.T., Doucet D., New Temperature Dependent Thermal Conductivity Data for Water-based Nanofluids, *International Journal of Thermal Sciences*, **48(2):** 363–371 (2009).

[43] Maïga S.E.B., Nguyen C.T., Galanis N., Roy G., Heat Transfer Behaviours of Nanofluids in a Uniformly Heated Tube, *Super. Micro.*, **35(3–6):** 543–557 (2004).

[44] Brinkman H.C., The Viscosity of Concentrated Suspensions and Solutions, *The Journal of Chemical Physics*, **20(4):** 571–571 (1952).

[45] Bidarmaghz A., Narsilio G.A., Is Natural Convection within an Aquifer a Critical Phenomenon in Deep Borehole Heat Exchangers' Efficiency?, *Applied Thermal Engineering*, **212:** 118450 (2022).

[46] Huang Y., Zhang Y., Xie Y., Zhang Y., Gao X., Ma J., Long-Term Thermal Performance Analysis of Deep Coaxial Borehole Heat Exchanger based on Field Test, *J. Clean. Produc.*, **278:** 123396 (2021).

[47] Zhang L., Shi Z., Yuan T., Study on the Coupled Heat Transfer Model based on Groundwater Advection and Axial Heat Conduction for the Double U-Tube Vertical Borehole Heat Exchanger, *Sustainability*, **12(18):** 7345 (2020).

[48] Basok B., Davydenko B., Koshlak H., Novikov V., Free Convection and Heat Transfer in Porous Ground Massif during Ground Heat Exchanger Operation, *Materials*, **15(14):** 4843 (2022).

[49] Mehrpooya M., Asadbeigi M., Ghafoorian F., Farajyar S., Investigation and Optimization on Effective Parameters of a H-rotor Darrieus Wind Turbine, Using CFD Method, *Iranian Journal of Chemistry and Chemical Engineering (IJCCE)*, **42(9):** 3030-3046 (2023).

[50] Akhlagi M., Ghafoorian F., Mehrpooya M., Sharifi Rizi M., Effective Parameters Optimization of a Small Scale Gorlov Wind Turbine, Using CFD Method, *Iranian Journal of Chemistry and Chemical Engineering (IJCCE)*, **42(7):** 2286-2304 (2023).

Research Article